Bugg, C. E., & Sternglanz, H. (1974) in *Molecular and Quantum Pharmacology* (Bergmann, E., & Pullman, B., Eds.) pp 473–500, D. Reidel, Dordrecht, Holland.
Driggers, P. H., & Beattie, K. L. (1988a) *J. Biol. Chem.* (submitted for publication).
Driggers, P. H., & Beattie, K. L. (1988b) *J. Mol. Biol.* (submitted for publication).
Freese, E. (1959) *J. Mol. Biol. 1*, 87–105.
Hillebrand, G. G., & Beattie, K. L. (1985) *J. Biol. Chem. 260*, 3116–3125.
Hillebrand, G. G., McCluskey, A. H., Abbott, K. A., Revich, G. G., & Beattie, K. L. (1984) *Nucleic Acids Res. 12*, 3155–3171.
Hunter, W. N., Brown, T., Anand, N. N., & Kennard, O. (1986) *Nature (London) 320*, 552–555.
Joyce, C. J., & Grindley, N. D. F. (1983) *Proc. Natl. Acad. Sci. U.S.A. 80*, 1830–1834.
Katritzky, A. R., & Waring, A. J. (1962) *J. Chem. Soc.*, 1540–1544.
Lawley, P. D., & Brookes, P. D. (1962) *J. Mol. Biol. 4*, 216–219.
Revich, G. G., Hillebrand, G. G., & Beattie, K. L. (1984) *J. Chromatogr. 317*, 283–300.
Sowers, L. C., Fazakerley, G. V., Kim, H., Dalton, L., & Goodman, M. F. (1986a) *Biochemistry 25*, 3983–3988.
Sowers, L. C., Fazakerley, G. V., Eritja, R., Kaplan, B. E., & Goodman, M. F. (1986b) *Proc. Natl. Acad. Sci. U.S.A. 83*, 5434–5438.
Sternglanz, H., & Bugg, C. E. (1975) *Biochim. Biophys. Acta 378*, 1–11.
Uhl, W., Reiner, J., & Gassen, H. G. (1983) *Nucleic Acids Res. 11*, 1167–1180.
Watson, J. D., & Crick, F. H. C. (1953) *Nature (London) 171*, 737–738.

Refinement of the Solution Structure of the Ribonucleotide 5′r(GCAUGC)$_2$: Combined Use of Nuclear Magnetic Resonance and Restrained Molecular Dynamics†

Claudia Scalfi Happ, Erwin Happ, Michael Nilges, Angela M. Gronenborn,*,‡ and G. Marius Clore*,‡
Max-Planck-Institut für Biochemie, D-8033 Martinsried bei München, FRG
Received August 17, 1987; Revised Manuscript Received October 30, 1987

ABSTRACT: The solution structure of the self-complementary hexamer 5′r(GCAUGC)$_2$ is investigated by means of nuclear magnetic resonance spectroscopy and restrained molecular dynamics. The proton resonances are assigned in a sequential manner, and a set of 110 approximate interproton distance restraints are derived from the two-dimensional nuclear Overhauser enhancement spectra. These distances are used as the basis of a structure refinement by restrained molecular dynamics in which the experimental restraints are incorporated into the total energy function of the system in the form of effective potentials. Eight restrained molecular dynamics simulations are carried out, four starting from a structure with regular A-type geometry and four from one with regular B-type geometry. The atomic root mean square (rms) difference between the initial structures is 3.2 Å. In the case of all eight simulations, convergence is achieved both globally and locally to a set of very similar A-type structures with an average atomic rms difference between them of 0.8 ± 0.2 Å. Further, the atomic rms differences between the restrained dynamics structures obtained by starting out from the same initial structures but with different random number seeds for the assignment of the initial velocities are the same as those between the restrained dynamics structures starting out from the two different initial structures. These results suggest that the restrained dynamics structures represent good approximations of the solution structure. The converged structures exhibit clear sequence-dependent variation in some of the helical parameters, in particular helix twist, roll, slide, and propellor twist. The variation in roll follows that predicted by Dickerson [Dickerson, R. E. (1983) *J. Mol. Biol. 166*, 419–441], whereas those for helix twist and propellor twist follow the opposite trend to the predicted one.

As part of a study on the conformations of nucleic acids in solution we present a combined nuclear magnetic resonance (NMR)[1] and restrained molecular dynamics study on the self-complementary RNA hexamer 5′r(GCAUGC)$_2$. This particular sequence was chosen to enable a direct structural comparison with the analogous DNA oligonucleotide 5′d-(GCATGC)$_2$, whose three-dimensional structure had previously been determined by the same methods (Nilges et al., 1987a). We first assign the resonances of the RNA hexamer in a sequential manner using a combination of HOHAHA and NOESY spectroscopy; a set of approximate interproton distance restraints is then derived from the NOESY cross-peak

† This work was supported by the Max-Planck Gesellschaft, Grant C1 86/1-1 from the Deutsche Forschungsgemeinschaft, and Grant 321/4003/0318909A from the Bundesministerium für Forschung und Technologie (G.M.C. and A.M.G.).
‡ Present address: Laboratory of Chemical Physics, Building 2, National Institute of Diabetes and Digestive and Kidney Disorders, National Institutes of Health, Bethesda, MD 20892.

[1] Abbreviations: NMR, nuclear magnetic resonance; NOE, nuclear Overhauser effect; NOESY, two-dimensional NOE spectroscopy; HOHAHA, two-dimensional homonuclear Hartmann–Hahn spectroscopy; rms, root mean square; RD, restrained dynamics.

0006-2960/88/0427-1735$01.50/0

intensities and used as the basis of a structure refinement by restrained molecular dynamics (Clore et al., 1985a, 1986; Kaptein et al., 1985; Brünger et al., 1986; Nilsson et al., 1986). As in previous studies on two DNA hexamers (Nilsson et al., 1986; Nilges et al., 1987a) and a DNA decamer (Nilges et al., 1987b), convergence is achieved by starting from two quite different initial structures, namely, structures with regular A- and B-type geometries. The converged structures are analyzed and shown to exhibit sequence-dependent variations in the value of helical parameters, some of which are different from those found in the analogous DNA hexamer.

Experimental Procedures

Sample Preparation. The RNA hexamer 5′r(GCAUGC)$_2$ was synthesized in solution by condensation of two trimer blocks as described previously (Happ et al., 1987). After being deblocked in three consecutive steps, the fully deprotected product was purified by ion-exchange chromatography on DEAE-Sephadex A-25 under denaturing conditions. The hexamer was desalted on a Baker-10 SPE reverse-phase C18 column and finally on Sephadex G-25. Electrophoresis on a 20% polyacrylamide gel confirmed the purity of the isolated compound.

After extensive freeze-drying, the hexamer was dissolved unbuffered in either 99.995% D_2O or 90% H_2O/10% D_2O to give a final concentration of 7.5 mM. Note that some Na^+ counterions are present as the cations bound tightly to the phosphate groups are not removed in the desalting procedure. All glassware was heated at 180 °C overnight to inactivate all possible traces of ribonucleases.

The temperature used for all NMR experiments was 10 °C; under these conditions the hexamer was entirely double stranded as judged by the observation of three imino proton resonances in 90% H_2O/10% D_2O.

NMR Spectroscopy. All NMR spectra were recorded on a Bruker AM500 spectrometer. Two-dimensional NOESY (Jeener et al., 1979; Macura et al., 1982) and MLEV17 HOHAHA spectra (Davis & Bax, 1985; Bax & Davis, 1985) were recorded in pure-phase absorption mode with the time-proportional incrementation method (Redfield & Kuntz, 1975; Bodenhausen et al., 1980; Marion & Wüthrich, 1983). To reduce t_1 noise, the first time domain data points were multiplied by a factor of 0.5 (Otting et al., 1986). Base-line correction (Pearson, 1977) was carried out after the first and second transforms. Quantification of the NOESY cross-peak intensities was carried out on a VAX 11/780 by determination of the volume of each cross-peak by two-dimensional integration with a modified version of the Groningen 2D NMR processing program (Boelens, Kaptein, and Scheek, unpublished data).

Restrained Molecular Dynamics. All energy minimization and molecular dynamics calculations were carried out on a CONVEX-C1XP computer using the program XPLOR (Brünger et al., 1987a,b; A. T. Brünger et al., unpublished data) which is derived from the program CHARMM (Brooks et al., 1983) and has been especially adapted for restrained molecular dynamics. The energy function used comprises an all-hydrogen empirical energy function ($E_{empirical}$) developed for nucleic acids (Nilsson & Karplus, 1985) and effective interproton distance (E_{NOE}) and torsion angle (E_ϕ) restraint energy functions. The effective NOE restraint potential, E_{NOE}, has the form of a skewed biharmonic potential (Clore et al., 1985) given by

$$E_{NOE}(r_{ij}) = \begin{cases} c_1(r_{ij} - r_{ij}^0)^2 & \text{if } r_{ij} > r_{ij}^0 \\ c_2(r_{ij} - r_{ij}^0)^2 & \text{if } r_{ij} < r_{ij}^0 \end{cases} \quad (1)$$

where r_{ij} and r_{ij}^0 are the calculated and experimental distances, respectively, and c_1 and c_2 are force constants given by

$$c_1 = k_B TS/2(\Delta_{ij}^+)^2 \qquad c_2 = k_B TS/2(\Delta_{ij}^-)^2 \quad (2)$$

where k_B is the Boltzmann constant, T is the absolute temperature, S is a scale factor, and Δ_{ij}^+ and Δ_{ij}^- are the positive and negative error estimates on the value of r_{ij}^0. The effective torsion angle restraint potential has the form of a square well given by (Clore et al., 1986b)

$$E_\phi = \begin{cases} c(\phi_{ij} - \phi_{ij}^u)^2 & \text{if } \phi_{ij} > \phi_{ij}^u \\ 0 & \\ c(\phi_{ij} - \phi_{ij}^l)^2 & \text{if } \phi_{ij} < \phi_{ij}^l \end{cases} \quad (3)$$

where c is a force constant, ϕ_{ij} is the calculated value of the torsion angle, and ϕ_{ij}^u and ϕ_{ij}^l are the upper and lower experimental limits of the torsion angle. With respect to the electrostatic component of the empirical energy function, the effect of solvent was approximated by a $1/r$ screening function (Gelin & Karplus, 1977; Brooks et al., 1983) and by reducing the net charge on the phosphate group to $-0.32e$ (Tidor et al., 1982). The nonbonded interactions were switched off, by use of a cubic switching function, between 9.5 and 10.5 Å, with pairs up to 11.5 Å included in the nonbonded list. Integration of the classical equations of motion was performed by a Verlet integration algorithm (Verlet, 1967) with initial velocities assigned from a Maxwellian distribution at 400 K. The temperature of the system was maintained constant by rescaling the velocities of the atoms energy 0.1 ps. The time step of the integrator was 0.001 ps, and the nonbonded interaction lists were updated every 0.02 ps. Bond lengths involving hydrogen atoms were kept fixed with the SHAKE algorithm (Ryckaert et al., 1977).

Structural Analysis. Displaying of trajectories was carried out on an Evans & Sutherland PS390 color graphics system using a modified version of the function network of FRODO (Jones, 1978) interfaced with XPLOR. Analysis of helical parameters was carried out by the program HETRAN (M. Nilges and G. M. Clore, unpublished data), which is a modified version of the programs AHELIX (written by J. Rosenberg) and BROLL and CYLIN (written by R. E. Dickerson) adapted to deal with dynamics trajectories (Nilges et al., 1987a).

Results and Discussion

Sequential Resonance Assignment and Interproton Distances. The assignment of the nonexchangeable protons was accomplished in a sequential manner (Reid et al., 1983; Scheek et al., 1983; Hare et al., 1983; Clore & Gronenborn, 1983, 1985a) by (a) Hartmann–Hahn spectroscopy to demonstrate direct and relayed through-bond connectivities along the H1′ ↔ H2′ ↔ H3′ ↔ H4′ ↔ H5′/H5″ pathway within each sugar unit and (b) NOESY spectroscopy to demonstrate through-space (<5 Å) connectivities along the H1′/H2′/H3′(i − 1) ↔ H8/H6(i) ↔ H1′/H2′/H3′(i) pathway. Some examples of NOESY spectra are shown in Figure 1, and the complete list of assignments is given in Table I.

Interproton distances were determined from the intensities of the cross-peaks in the 100-ms NOESY spectra with the C(H5)–C(H6) and U(H5)–U(H6) distances (2.5 Å) and cross-peak intensities as internal references from (Wagner & Wüthrich, 1979; Dobson et al., 1982; Clore & Gronenborn, 1985b)

$$\langle r_{ij}^{-6}\rangle^{-1/6} = [a_{H5\text{-}H6}(\tau_m)/a_{ij}(\tau_m)]^{-1/6} r_{H5\text{-}H6} \quad (4)$$

[where r_{ij} and $a_{ij}(\tau_m)$ are the distance and NOE cross-peak intensity at a mixing time τ_m, respectively, between protons

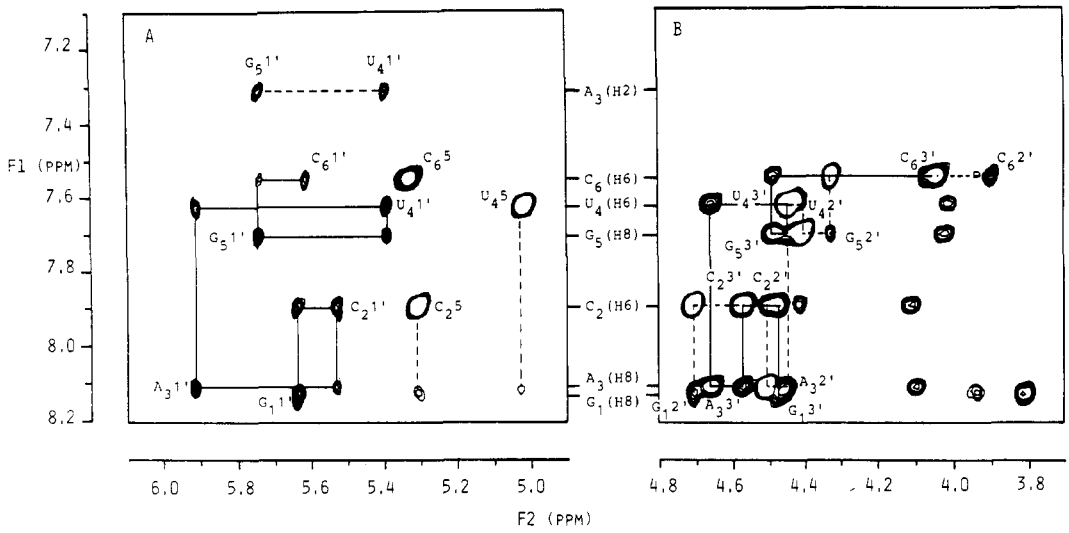

FIGURE 1: (A) H8/H6(F1 axis)–H1'/H5(F2 axis) and (B) H8/H6(F1 axis)–H2'/H3'/H4'/H5'/H5''(F2 axis) of the 100-ms NOESY spectrum of the RNA hexamer in D_2O. H1'($i-1$) ↔ H8/H6(i) ↔ H1'(i) and H3'($i-1$) ↔ H8/H6(i) ↔ H3'(i) connectivities are shown in (A) and (B), respectively, as solid lines (—); H2'($i-1$) ↔ H8/H6(i) ↔ H2'(i) connectivities are shown in (B) as interrupted lines (– –).

Table I: Proton Resonance Assignments of the RNA Hexamer at 10 °C

	chemical shift (ppm)							
residue	H8/H6	H5/H2	H1/H3	H1'	H2'	H3'	H4'	H5',H5''
G_1	8.08		12.75	5.64	4.71	4.48	4.24	3.94, 3.81
C_2	7.83	5.31		5.53	4.52	4.58	4.40	4.11
A_3	8.05	7.25		5.91	4.46	4.66	4.67	4.10
U_4	7.56	5.02	13.42	5.40	4.41	4.46	4.44	4.01
G_5	7.65		12.65	5.75	4.33	4.49	4.38	4.03
C_6	7.49	5.33		5.62	3.90	4.05	4.06	3.94

i and *j*] on the assumption that the effective correlation times of the *i*–*j* and intranucleotide H5–H6 interproton vectors are about the same and that the initial rate condition is approximately valid. The validity of the latter assumption at a mixing time of 100 ms was verified by selective one-dimensional experiments using the NOESY pulse sequence with the first nonselective 90° pulse replaced by a selective 90° Gaussian-shaped pulse (Kessler et al., 1986).

In using eq 4 the effects of spin–diffusion and variations of the effective correlation time on the estimated distance values should be considered. From model calculations (Clore & Gronenborn, 1985b) and considerations of RNA stereochemistry (Clore et al., 1985b), it can be deduced that under the experimental conditions employed no distortions of cross-peak intensities will occur for $r_{ij} < 3$ Å and only minimal distortions giving rise to distance errors of <0.2 Å will occur for 3 Å < $r_{ij} < 4$ Å. No variation in effective correlation time for the three intraresidue H5–H6 vectors could be detected. Although the effective correlation time of the intraresidue H2'–H2'' sugar vector in DNA oligonucleotides is a factor of approximately 3 times shorter than that of the intranucleotide H5–H6 base vector (Clore & Gronenborn, 1984; Nilges et al., 1987a,b), there appears to be no significant difference between the effective correlation times of sugar and base vectors in RNA (Clore et al., 1985b). Despite the fact that there is no readily available fixed distance vector within the ribose ring (the H5'–H5'' vector not being suitable due to severe spectral overlap), the comparable effective correlation times for the sugar and base vectors are easily checked by calculation of the H1'–H2' distance with the H5–H6 vector as an internal reference. The H1'–H2' distance has a minimum value of ~2.5 Å when the sugar pucker is in the 3'-endo conformation characteristic of A-RNA and a maximal value of ~2.9 Å when the sugar pucker is in the 2'-endo conformation. The values obtained for the hexamer with eq 4 all lie in the range 2.5–2.7 Å. If the effective correlation time of the sugar vectors were significantly shorter than that of the bases, these values would represent overestimates, which clearly cannot be the case on stereochemical grounds.

A summary of the calculated interproton distances is given in Table II. Taking into account both the considerations discussed above as well as the errors involved in determining cross-peak intensities by volume integration, we estimate that the errors are –0.2 Å/+0.3 Å for $r_{ij} < 3$ Å and –0.3 Å/+0.4 Å for 3 Å ≤ $r_{ij} < 5$ Å.

Information on the C4'–C3' (δ) bond torsion angle was also deduced from $^3J_{1'2'}$ coupling constants. From the one-dimensional spectrum, these could easily be estimated to be less than 3 Hz for all ribose units, indicative of a value of $\delta < 90°$ (Altona & Sunderalinguam, 1972; Davies, 1985).

Structure Refinement. In order to obtain the structure of the hexamer in solution, we proceeded to carry out restrained molecular dynamics calculations incorporating the experimental interproton distance and δ torsion angle data into the total energy of the system in the form of effective potentials (cf. eq 1 and 3). Two initial structures were used: an A-type structure known as IniA and a B-type one known as IniB. The Cartesian coordinates for these structures were generated from the polar coordinates for classical A- and B-DNA obtained from fiber diffraction data (Arnott & Hukins, 1972). The atomic rms difference between the two initial structures is 3.2 Å. The calculations proceeded in three stages: (i) 8 ps of quenched restrained dynamics at 400 K in which the velocities were rescaled to 400 K every 0.1 ps, and the NOE restraint scale factor S (cf. eq 1 and 2) was increased from 0.32 up to a maximum value of 8.0 and the δ torsion angle restraint force constant from 0.63 kcal mol^{-1} rad^{-2} up to a maximum value of 40 kcal mol^{-1} rad^{-2} by multiplying their respective values by $10^{0.2}$ every 0.1 ps (the values of the NOE and δ restraint force constants reached at the end of this stage were main-

Table II: $\langle r^{-6}\rangle^{-1/6}$ Mean Interproton Distances Derived from the 100-ms NOESY Spectra[a]

(A) Intranucleotide

proton	r_{ij} (Å) C_1	G_2	A_3	U_4	G_5	C_6
sugar–sugar						
H1′–H2′	2.6	2.6	2.5	2.6	2.7	2.6
H1′–H4′	3.1	3.2	3.3	3.2	3.1	3.0
sugar–base						
H1′–H6/H8	3.7	3.8	3.7	3.5	3.6	3.7
H2′–H6/H8	3.4		3.3		3.9	3.3
H3′–H6/H8	3.0	2.6	2.9	*b*	2.9	2.7
H5′/H5″–H6/H8[c]	3.1	3.3	3.3	3.5	3.2	

(B) Internucleotide (Intrastrand)

proton of 5′-residue	proton of 3′-residue	r_{ij} (Å) G_1pC_2	C_2pA_3	A_3pU_4	U_4pG_5	G_5pC_6
H1′	H6/H8	3.6	4.1	4.0	3.9	4.0
H2′	H6/H8	2.5	2.4	*b*	2.3	2.6
H3′	H6/H8	2.7	3.0	3.0		3.2
H2′	H5	3.3		2.9		
H3′	H5	2.9		3.1		
H8/H6	H5	4.2		3.8		
H2	H1′			3.5		

(C) Internucleotide (Interstrand)

proton	r_{ij} (Å)
A_3(H2)–G_{11}(H1′)/A_9(H2)–G_5(H1′)	3.3
A_3(H2)–U_{10}(H3)/A_9(H2)–U_4(H3)	2.9

[a] The estimated errors in the distances are as follows: $-0.2/+0.3$ Å for $r_{ij} < 3$ Å and $-0.3/+0.4$ Å for 3 Å $\leq r_{ij} \leq 5$ Å (see text). [b] The A_3(H2′) and U_4(H3′) resonances are superimposed. Consequently, the A_3(H2′)–U_4(H6) and U_4(H3′)–U_4(H6) cross-peaks are superimposed. The integrated cross-peak intensity of this peak corresponds to a distance of 2.2 Å. In the restraints list, we set this value equal to the $\langle r^{-6}\rangle^{-1/6}$ average of the two corresponding distances. [c] As the H5′ and H5″ resonances were not stereospecifically assigned, the distances given in the table were set equal to the $\langle r^{-6}\rangle^{-1/6}$ average of the $r_{H5'-H6/H8}$ and $r_{H5''-H6/H8}$ distances.

Table III: Atomic rms Differences between Initial and Final Structures[a]

	atomic rms difference (Å)		atomic rms difference (Å)
Initial Structures		rms Distributions	
IniA vs IniB	3.21	⟨RDA⟩ vs ⟨RDA⟩	0.72 ± 0.27
		⟨RDB⟩ vs ⟨RDB⟩	0.85 ± 0.16
rms Shifts		⟨RDA⟩ vs ⟨RDB⟩	0.80 ± 0.20
IniA vs ⟨RDA⟩	1.67 ± 0.13	⟨RD⟩ vs ⟨RD⟩	0.80 ± 0.21
IniB vs ⟨RDB⟩	2.89 ± 0.24	⟨RD⟩ vs $\overline{RD}$	0.54 ± 0.11
$\overline{RD}$ vs ($\overline{RD}$)m	0.15	⟨RD⟩ vs ($\overline{RD}$)m	0.56 ± 0.12

[a] The notation of the structures is as follows: IniA and IniB are the initial structures with regular A and B geometries, respectively. ⟨RDA⟩ are the four final structures derived from IniA and ⟨RDB⟩ the four final structures derived from IniB; ⟨RD⟩ refers to all eight converged structures (i.e., ⟨RDA⟩ and ⟨RDB⟩ collectively); $\overline{RD}$ is the mean structure obtained by averaging the coordinates of the eight converged structures; ($\overline{RD}$)m is the structure obtained by restrained energy minimization of the mean structure $\overline{RD}$. The atomic standard rms error in the coordinates of the average structure $\overline{RD}$ is given by rmsd/$\sqrt{8}$ ~ 0.19 Å, where rmsd is the average atomic rms difference between the eight ⟨RD⟩ structures and the mean structure $\overline{RD}$.

Table IV: rms Interproton Distance Deviations, Deviations from Ideality, and Restraints and Nonbonding Energies for Initial and Final Structures

	rms interproton distance deviations (Å)			
structure	all (126)	intraresidue (66)	interresidue (44)	base pairing (16)[a]
IniA	0.40	0.20	0.58	0.16
IniB	1.03	0.81	1.42	0.15
⟨RDA⟩	0.20 ± 0.002	0.15 ± 0.005	0.29 ± 0.01	0.056 ± 0.005
⟨RDB⟩	0.20 ± 0.005	0.15 ± 0.005	0.28 ± 0.005	0.060 ± 0.003
$\overline{RD}$	0.20	0.14	0.29	0.062
($\overline{RD}$)m	0.20	0.15	0.28	0.052

	deviations from ideality[b]		
structure	bonds (Å) (412)	angles (deg) (732)	impropers (deg) (172)
IniA	0.008	3.18	0.33
IniB	0.011	3.09	0.31
⟨RDA⟩	0.008 ± 0	3.64 ± 0.005	0.26 ± 0.02
⟨RDB⟩	0.008 ± 0	3.68 ± 0.02	0.27 ± 0.005
$\overline{RD}$	0.097	10.89	4.90
($\overline{RD}$)m	0.008	5.13	0.28

	restraint energy (kcal/mol)		nonbonding energy (kcal/mol)		
structure	E_{NOE}[d]	E_δ[e]	van der Waals	electrostatic	H bond
IniA	623	0	−27	−104	−40
IniB	3008	866	2203	−398	−35
⟨RDA⟩	117±4	0.006 ± 0.004	−195 ± 2	−181 ± 4	−68 ± 5
⟨RDB⟩	117±4	0.007 ± 0.009	−197 ± 2	−184 ± 5	−69 ± 5
$\overline{RD}$	139	0.002	−193	−157	−56
($\overline{RD}$)m	120	0.004	−197	−170	−61

[a] In addition to the experimental interproton distance restraints, a set of 16 base-pairing restraints corresponding to the base-pair hydrogen bonds were added to the NOE restraint energy function. These are as follows: for A·U base pairs $r_{A(NG)-U(O4)}$ = 2.95 Å and $r_{A(N1)-U(H3)}$ = 2.82 Å; for G·C base pairs $r_{G(O6)-C(N4)}$ = 2.91 Å, $r_{G(N1)-C(N3)}$ = 2.95 Å, and $r_{G(N2)-C(O2)}$ = 2.86 Å. The values were taken from the X-ray structure analyses of ApU (Seeman et al., 1976) and GpC (Rosenberg et al., 1976), and the error estimates for these values used in the calculations were ±0.2 Å. [b] Deviations from ideality indicate deviations from standard values for covalent geometry (i.e., bonds, angles, and planes). [c] The improper torsion angle restraints are the restraints used to maintain planarity; unlike conventional dihedral angle restraints, they have only one minimum described by a simple harmonic potential. [d] The scale factor S (cf eq 2) used in calculating the NOE restraint energy was 8. This corresponds to force constants of 59.6, 26.5, and 14.9 kcal mol^{-1} Å^{-2} for distance errors of 0.2, 0.3, and 0.4 Å, respectively. [e] The force constant for the δ torsion angle restraint was 40 kcal mol^{-1} rad^{-2}.

tained for the rest of the calculation); (ii) 12 ps of quenched restrained dynamics at 300 K in which the velocities were rescaled every 0.1 ps; (iii) 400 cycles of restrained energy minimization of the coordinates obtained by averaging the coordinate trajectories over the last 8 ps of the second stage. Four calculations were carried out from each initial structure with different random number seeds for the assignments of the initial velocities. Each calculation took approximately 5 h on the CONVEX-C1XP computer. The final structures obtained by starting from IniA are referred to as ⟨RDA⟩ and those starting from IniB as ⟨RDB⟩; ⟨RDA⟩ and ⟨RDB⟩ are also referred to collectively as ⟨RD⟩. The coordinates of the eight final structures were also averaged to yield the average structure $\overline{RD}$, which was subjected to 400 cycles of restrained energy minimization to produce the structure ($\overline{RD}$)m.

The atomic rms differences between the structures are given in Table III, and the rms differences between the calculated and experimental interproton distances, the deviations from ideality for bonds, angles, and planes, the NOE and δ restraint energies, and the nonbonding energies are given in Table IV. Superpositions of the two initial structures and of the final structures are shown in Figure 2 and plots of atomic rms difference between various structures as a function of residues number in Figure 3.

It is clear from the data in Tables II and III and Figures 2 and 3 that convergence to essentially the same structures, both globally and locally, has been achieved by starting from both initial structures. Further, the atomic rms differences

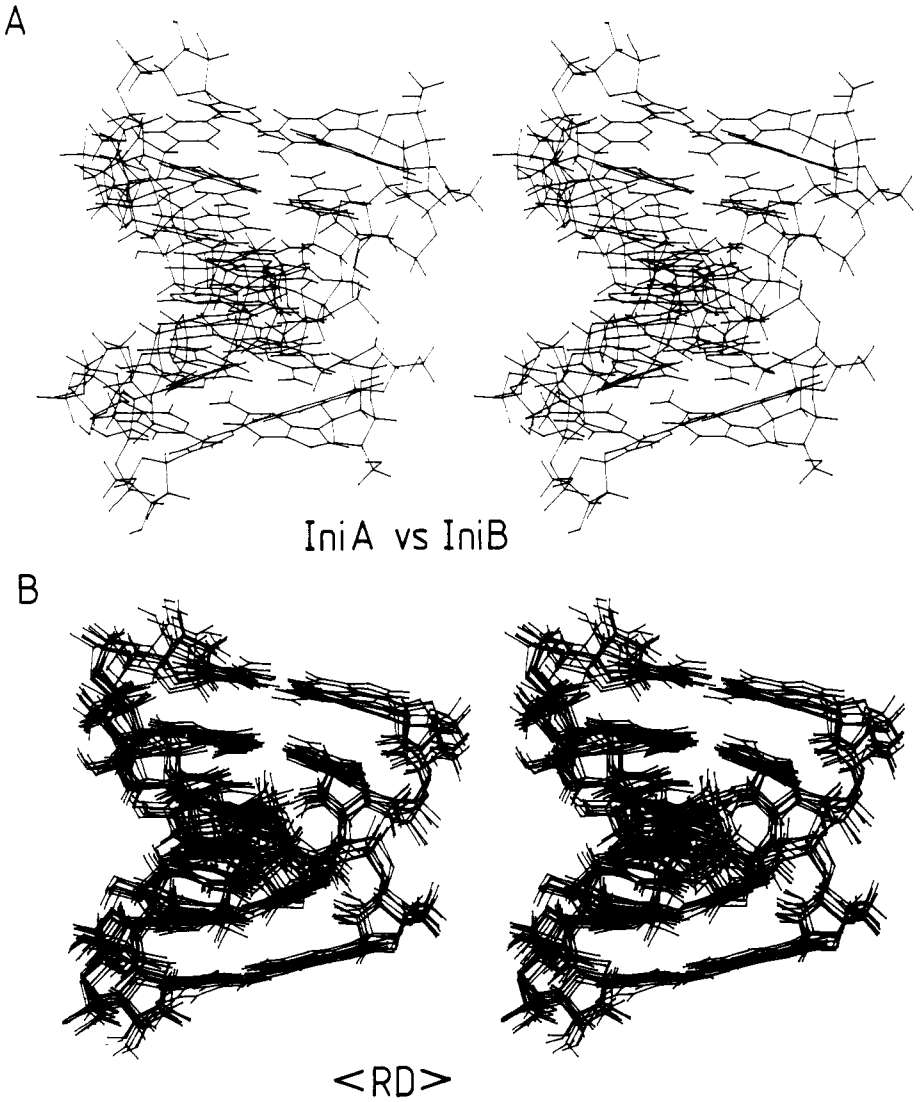

FIGURE 2: (A) Superposition of the two initial structures (IniA and IniB) and (B) superposition of the eight converged structures (⟨RD⟩).

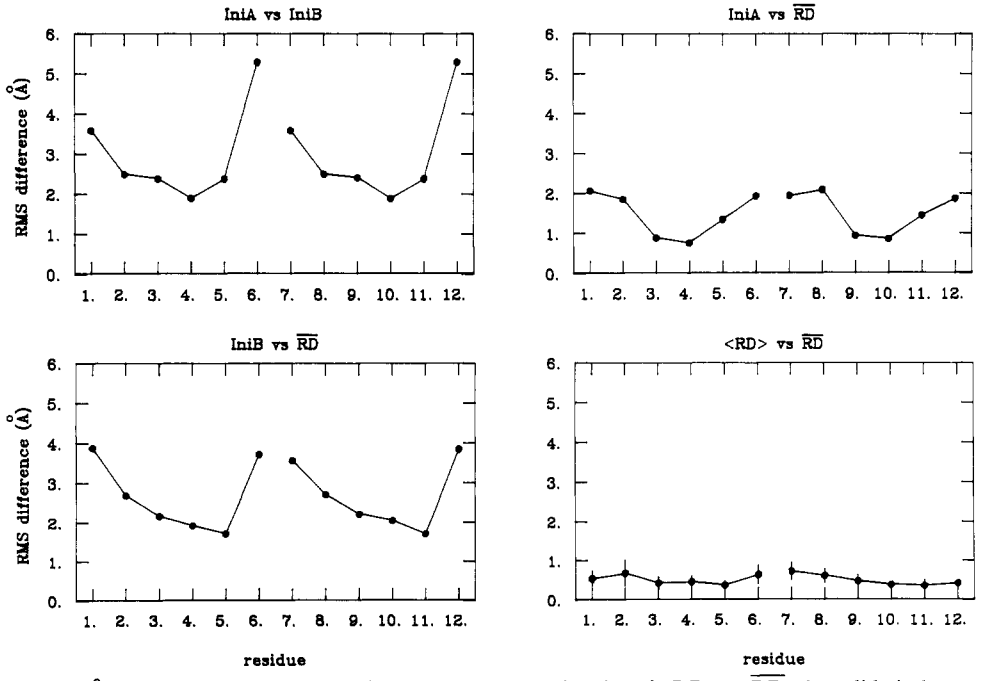

FIGURE 3: rms differences (Å) for all atoms between various structures. In the plot of ⟨RD⟩ vs $\overline{RD}$, the solid circles represent the average atomic rms difference and the bars the standard deviations in these values.

Table V: Average Values of Glycosidyl and Backbone Torsion Angles, Sugar Pucker Phase Angle, Helix Twist and Rise, and Base-Pair Inclination and Displacement for Initial and Final Structures

structure	glycosyl, χ (deg)	backbone torsion angles (deg)						phase (deg)[a]	helix twist (deg)	helix rise (Å)	inclination (deg)	displacement (Å)
		α	β	γ	δ	ϵ	ζ					
IniA	−154	−86	−151	47	83	178	−46	354	32.7	2.56	−19.3	4.49
IniB	−98	−47	−146	36	156	155	−95	173	36.0	3.38	5.9	−0.23
⟨RD⟩	−156 ± 5	−70 ± 15	175 ● 7	57 ● 2	85 ± 7	160 ± 3	−67 ± 5	345 ± 9	35 ± 7	2.7 ± 0.2	−12.4 ± 3.3	2.3 ± 0.5

[a] The sugar pucker phase angle is calculated as described by Cremer and Pople (1975) with the apex at atom 3 and C4′ = atom 0, C1′ = atom 1, and so on.

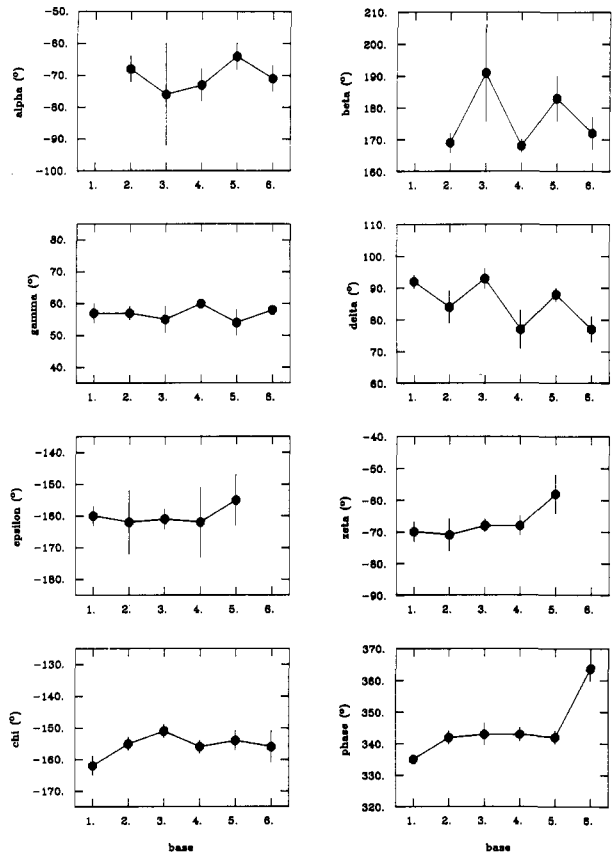

FIGURE 4: Variations in backbone and glycosidic bond torsion angles as well as in the phase angle describing the sugar pucker for the eight ⟨RD⟩ converged structures. The solid circles represent the average of the values for the eight converged structures and the bars the rms deviations in these values.

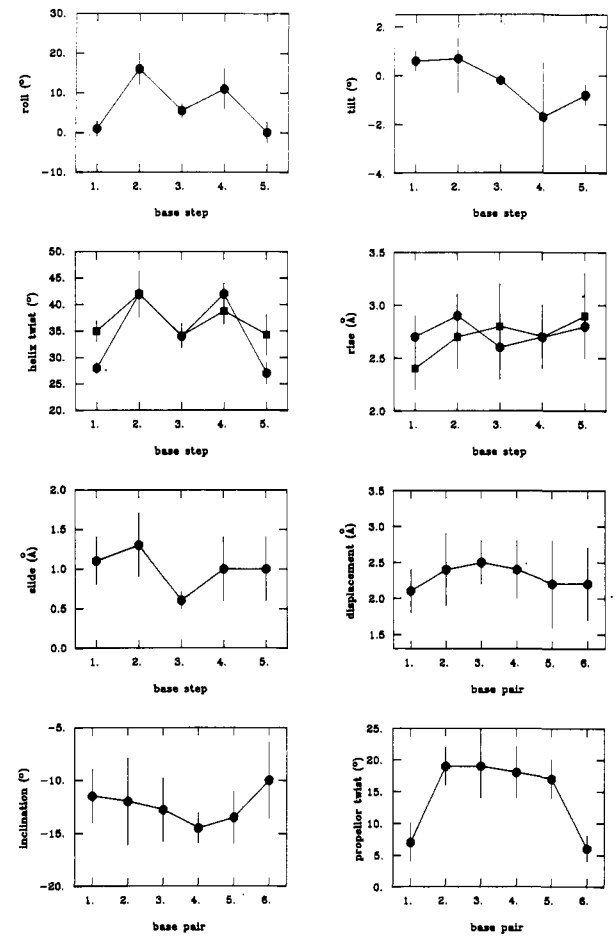

FIGURE 5: Variations in helical parameters for the eight ⟨RD⟩ converged structures. The solid circles and squares represent the average of the values for the eight converged structures and the bars the rms deviations in these values. In the case of helix twist and rise, the solid circles (●) represent the global helix twist and rise and the squares (■) the local helix twist and rise. The exact definitions of the various helical parameters are given by Dickerson (1983).

between the final structures are independent of the starting structures. Thus, the difference between the final structures arises from the different random number seeds used to assign the initial velocities. The average atomic rms difference between the final structures is ~0.8 Å and that between the final structures and the mean structure RD is ~0.5 Å, which is comparable to the atomic rms fluctuations of the atoms about their average positions. The rms difference in the interproton distances (~0.2 Å) is within the experimental errors specified, and the δ torsion angles lie within the target range. In addition, the extent of convergence can be assessed from the plots of backbone torsion angles (Figure 4) and helical parameters (Figure 5) as a function of residue number.

It should be noted that in the absence of experimental restraints (i.e., using the same dynamics protocol but with the force constants for the NOE and δ torsion angle restraints set to zero) convergence from the two starting structures does *not* occur. Indeed, the structures diverge (atomic rms difference of 5.5 Å), and the structure starting from IniA remains A type and that from IniB B type. Thus, as in the previous cases (Nilsson et al., 1986; Nilges et al., 1987a,b), convergence is entirely due to the incorporation of the experimental restraints into the total energy function of the system in the form of effective potentials, and the structural features that emerge are not in any way artifacts arising from the empirical energy function. The role of the latter is solely to ensure that the local stereochemistry and nonbonded interactions are approximately correct.

Structural Features. The average values of the torsion angles and various helical parameters for the initial and converged structures are given in Table V. The values exhibited by the converged structures are typical of A-RNA (Saenger, 1984). Particularly characteristic are the glycosidic bond (λ) and C4′–C3′ (δ) torsion angles, the helix rise, and the base-pair displacement and inclination.

In contrast to the analogous DNA hexamer 5′d(GCATGC)$_2$ (Nilges et al., 1987a), the extent of base to base variation in the backbone and glycosidic bond torsion angles is much less

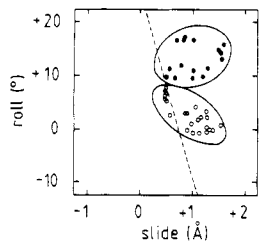

FIGURE 6: Roll–slide diagram for the eight ⟨RD⟩ converged structures. The closed circles represent the Pyr$_p$Pur steps and the open circles the Pur$_p$Pyr steps. The dashed line from roll, slide = −10°, 1 Å to +20°, 0.2 Å represents the break between A- and B-type DNA geometries, which lie to the right and left, respectively, of the line (Calladine & Drew, 1984).

marked. The helical parameters, however, show distinct variations. The variation in base roll, characterized by larger values for the Pyr$_p$Pur steps than for the Pur$_p$Pyr steps, is the same in the RNA and DNA hexamers and follows the trend predicted by Dickerson's (1983) sum function $\sum_2$. Slide is correlated with roll as it was in the case in the DNA hexamer. Most of the values in a roll–slide diagram (Figure 6) lie in the range characteristic of an A-type geometry (Calladine & Drew, 1984) and are grouped into two distinct clusters associated with Pyr$_p$Pur and Pur$_p$Pyr steps. The Pyr$_p$Pur cluster is located in a similar position to that found in the DNA hexamer, whereas the Pur$_p$Pyr one is shifted rightward along the slide axis into the A-type region. The variations in helix twist and propellor twist, however, follow opposite trends for the two oligonucleotides. Thus, in the case of the RNA hexamer the helix twist is increased at the Pyr$_p$Pur steps whereas it is decreased in the case of the DNA hexamer. Similarly, the propellor twist is decreased at residues 1 and 6 in the case of the RNA hexamer but decreased in the case of the DNA hexamer. The variation in helix twist and propellor twist in the RNA hexamer is thus anticorrelated with the trend predicted by Dickerson's (1983) sum functions $\sum_1$ and $\sum_4$, respectively.

Examination of the structure of the hexamer viewed down the helix axis (Figure 7) suggests that the structure is stabilized by near optimal base–base stacking. The Pur$_p$Pyr steps are

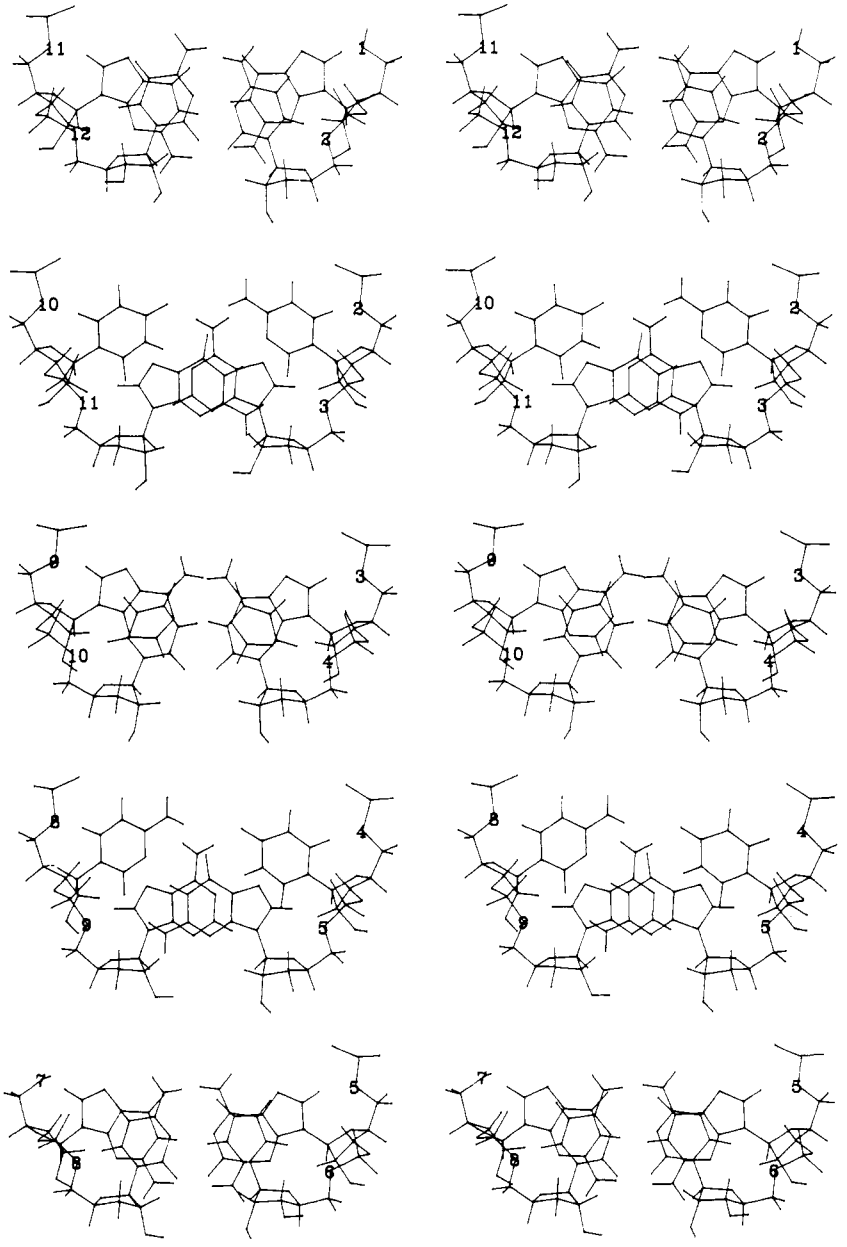

FIGURE 7: Stereoviews of the five individual base-pair steps of the restrained energy minimized average structure $(\overline{RD})$m viewed down the global helix axis.

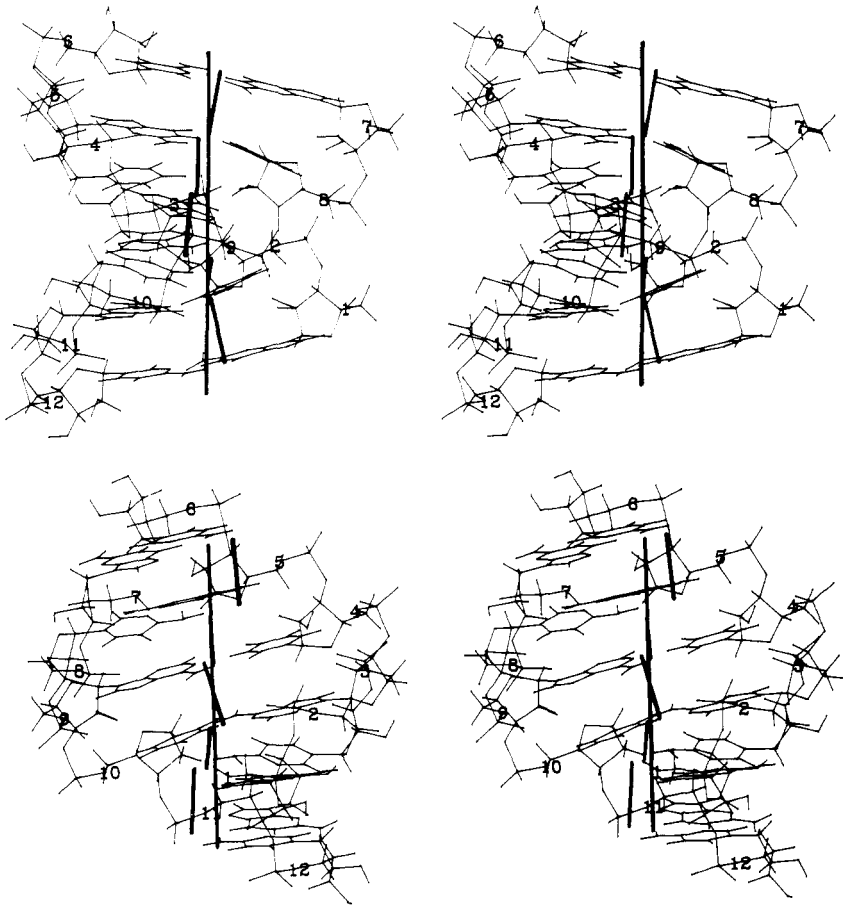

FIGURE 8: Two stereoviews of the average restrained energy minimized structure ($\overline{RD}$)m with the global and local helix axes superimposed.

characterized by almost perfect intrastrand stacking of the pyrimidine ring on the six-membered ring of the purine, whereas the Pyr_pPur steps are characterized by almost perfect interstrand stacking of the six-membered purine rings. This pattern of stacking is characteristic of A-RNA and even more so of A′-RNA (Saenger, 1984) and provides the structural basis for the experimental finding that stacking, as well as hydrogen bonding, is an important determinant of RNA stability (Turner et al., 1986).

One of the distinctive features of the DNA hexamer was its bent appearance with most of the bending occurring at the two Pyr_pPur steps (Nilges et al., 1987a). The global and local helix axes were at angles to each other, and the global axis represented a superhelix which the bent DNA wrapped around. These features are present in the RNA hexamer but to a much lesser degree. The global helix axis is located in the major groove (Figure 8). The local helix axes of base pair steps 2, 3, and 4 are slightly displaced inwards (i.e., in the direction of the minor groove) and at a small angle with respect to the global axis. The local axes for base pair steps 1 and 5 are slightly displaced toward the outside of the molecule. The local axes of steps 1 and 5 are at an angle of $\sim 20°$ to each other. This compares to a value of $\sim 50°$ in the case of the DNA hexamer. Thus, the extent of bending is much smaller in the RNA hexamer than in the DNA hexamer. That this is so can also be ascertained from the observation that the values for the local and global helix twist and for the local and global helical rise are very similar (Figure 5).

Concluding Remarks. In this paper we have shown that the restrained molecular dynamics can be successfully applied to RNA as well as to DNA. The structure of the RNA hexamer is of the A type. Although much more regular than DNA with regard to backbone torsion angles, distinct variations in the helical parameters are apparent. While base roll follows the same trend as in the analogous DNA hexamer, both helical twist and propellor twist follow opposite trends. We tentatively suggest that this pattern of variation is used to optimize intrastrand purine–pyrimidine stacking at Pur_pPyr steps and interstrand purine–purine stacking at Pyr_pPur steps.

Registry No. 5′r$(GCAUGC)_2$, 112506-39-5.

REFERENCES

Altona, C., & Sundaralinguam, M. (1972) *J. Am. Chem. Soc. 94*, 8205–8212.

Arnott, S., & Hukins, D. W. L. (1972) *Biochem. Biophys. Res. Commun. 47*, 1504–1509.

Bax, A., & Davis, D. G. (1985) *J. Magn. Reson. 65*, 355–360.

Bodenhausen, G., Vold, R. L., & Vold, R. R. (1980) *J. Magn. Reson. 37*, 93–106.

Brooks, B. R., Bruccoleri, R. E., Olafson, B. D., States, D. J., Swaminathan, S., & Karplus, M. (1983) *J. Comput. Chem. 74*, 187–217.

Brünger, A. T., Clore, G. M., Gronenborn, A. M., & Karplus, M. (1986) *Proc. Natl. Acad. Sci. U.S.A. 83*, 3801–3805.

Brünger, A. T., Kuriyan, J., & Karplus, M. (1987a) *Science (Washington, D.C.) 235*, 458–460.

Brünger, A. T., Clore, G. M., Gronenborn, A. M., & Karplus, M. (1987b) *Protein Engineer. 1*, 399–406.

Calladine, C. R., & Drew, H. R. (1984) *J. Mol. Biol. 178*, 773–782.

Clore, G. M., & Gronenborn, A. M. (1983) *EMBO J. 2*, 2109–2115.

Clore, G. M., & Gronenborn, A. M. (1984) *FEBS Lett. 172*, 219–225.

Clore, G. M., & Gronenborn, A. M. (1985a) *FEBS Lett. 179*, 187–198.

Clore, G. M., & Gronenborn, A. M. (1985b) *J. Magn. Reson. 61*, 158–164.
Clore, G. M., Gronenborn, A. M., Brünger, A. T., & Karplus, M. (1985a) *J. Mol. Biol. 186*, 435–455.
Clore, G. M., Gronenborn, A. M., & McLaughlin, L. W. (1985b) *Eur. J. Biochem. 151*, 153–165.
Clore, G. M., Brünger, A. T., Karplus, M., & Gronenborn, A. M. (1986a) *J. Mol. Biol. 191*, 523–551.
Clore, G. M., Nilges, M., Sukumaran, D. K., Brünger, A. T., Karplus, M., & Gronenborn, A. M. (1986b) *EMBO J. 5*, 2729–2735.
Cremer, D., & Pople, J. A. (1975) *J. Am. Chem. Soc. 97*, 1358–1367.
Davies, D. B. (1985) *Prog. Nucl. Magn. Reson. Spectrosc. 12*, 135–225.
Davis, D. G., & Bax, A. (1985) *J. Am. Chem. Soc. 107*, 2821–2822.
Dickerson, R. E. (1983) *J. Mol. Biol. 166*, 419–441.
Dobson, C. M., Olejniczak, E. T., Poulsen, F. M., & Ratcliffe, R. G. (1982) *J. Magn. Reson. 48*, 87–110.
Gelin, G. R., & Karplus, M. (1975) *Proc. Natl. Acad. Sci. U.S.A. 72*, 2002–2006.
Happ, E., Scalfi Happ, C., Clore, G. M., & Gronenborn, A. M. (1987) *Nucleic Acids Symp. Ser. 18*, 265–268.
Hare, D. R., Wemmer, D. E., Chou, S. H., Drobny, G., & Reid, B. R. (1983) *J. Mol. Biol. 171*, 319–336.
Jeener, J., Meier, B. H., Backmann, P., & Ernst, R. R. (1979) *J. Chem. Phys. 71*, 4546–4553.
Jones, T. A. (1978) *J. Appl. Crystallogr. 11*, 268–272.
Kaptein, R., Zuiderweg, E. R. P., Scheek, R. M., Boelens, R., & van Gunsteren, W. F. (1985) *J. Mol. Biol. 182*, 179–182.
Kessler, H., Oschkinat, H., Griesinger, C., & Bermerl, W. (1986) *J. Magn. Reson. 70*, 106–133.
Macura, S., Huang, Y., Suter, D., & Ernst, R. R. (1981) *J. Magn. Reson. 43*, 259–281.
Marion, D., & Wüthrich, K. (1983) *Biochem. Biophys. Res. Commun. 113*, 967–974.
Nilges, M., Clore, G. M., Gronenborn, A. M., Brünger, A. T., Karplus, M., & Nilsson, L. (1987a) *Biochemistry 26*, 3718–3733.
Nilges, M., Clore, G. M., Gronenborn, A. M., Piel, N., & McLaughlin, L. W. (1987b) *Biochemistry 26*, 3734–3744.
Nilsson, L., & Karplus, M. (1986) *J. Comput. Chem. 7*, 691–716.
Nilsson, L., Clore, G. M., Gronenborn, A. M., Brünger, A. T., & Karplus, M. (1986) *J. Mol. Biol. 188*, 455–475.
Otting, G., Widmer, W., Wagner, G., & Wüthrich, K. (1986) *J. Magn. Reson. 66*, 187–193.
Pearson, G. A. (1977) *J. Magn. Reson. 27*, 265–272.
Redfield, A. G., & Kuntz, S. D. (1975) *J. Magn. Reson. 19*, 250–254.
Reid, D. G., Salisbury, S. A., Bellard, S., Shakked, Z., & Williams, D. H. (1983) *Biochemistry 22*, 2019–2025.
Rosenberg, J. M., Seeman, N. C., Day, R. O., & Rich, A. (1976) *J. Mol. Biol. 104*, 145–167.
Ryckaert, J. P., Cicotto, G., & Berendsen, H. J. C. (1977) *J. Comput. Phys. 23*, 327–337.
Saenger, W. (1984) *Principles of Nucleic Acid Structures*, Springer Verlag, New York.
Scheek, R. M., Russo, N., Boelens, R., Kaptein, R., & van Boom, J. H. (1983) *J. Am. Chem. Soc. 105*, 2914–2916.
Seeman, N. C., Rosenberg, J. M., Suddath, F. L., Kim, J. J. P., & Rich, A. (1976) *J. Mol. Biol. 104*, 109–144.
Tidor, B., Irikura, K., Brooks, B. R., & Karplus, M. (1983) *J. Biomol. Struct. Dyn. 1*, 231–252.
Turner, D. H., Freier, S. M., Sugimoto, N., Hickery, D. R., Jaeger, J. A., Sinclair, A., Alkema, D., Neilson, T., Caruthers, M. H., & Kierzek, R. (1986) in *Structure and Dynamics of RNA* (van Knippenberg, P. H., & Hilbers, C. W., Eds.) pp 1–13, NATO ASI Series, Plenum, New York.
Verlet, L. (1967) *Phys. Rev. 159*, 98–105.
Wagner, G., & Wüthrich, K. (1979) *J. Magn. Reson. 33*, 675–680.